RSC Advances

PAPER

Cite this: *RSC Adv.*, 2021, **11**, 4472

Two-dimensional conductive phthalocyanine-based metal–organic frameworks for electrochemical nitrite sensing†

Shun Lu,[a] Hongxing Jia,*[a] Matthew Hummel,[a] Yanan Wu,[b] Keliang Wang,[c] Xueqiang Qi[d] and Zhengrong Gu*[a]

Received 14th December 2020
Accepted 5th January 2021

DOI: 10.1039/d0ra10522h

rsc.li/rsc-advances

2D nickel phthalocyanine based MOFs (NiPc-MOFs) with excellent conductivity were synthesized through a solvothermal approach. Benefiting from excellent conductivity and a large surface area, 2D NiPc-MOF nanosheets present excellent electrocatalytic activity for nitrite sensing, with an ultra-wide linear concentration from 0.01 mM to 11 500 mM and a low detection limit of 2.3 μM, better than most reported electrochemical nitrite sensors. Significantly, this work reports the synthesis of 2D conductive NiPc-MOFs and develops them as electrochemical biosensors for non-enzymatic nitrite determination for the first time.

Nitrite (NO_2^-) is a common environmental contaminant that appears in the water, soil and other environments, and also serves as a kind of preservative for the food industry.[1,2] Nitrite-rich contaminants cause terrible impacts on the ecological environment and public health due to the unreasonable utilization/treatment with nitrites in the field of farming, food industry, and environmental protection.[3] Therefore, it is of great importance for the accurate determination of nitrite in the drinking water or pickled foods.[4] Moreover, the World Health Organization (WHO) has established a maximum limit of nitrite dosage of 65.2 μM (3 mg L^{-1}) in drinking water. So, a determination strategy with a highly sensitive, selectively and rapid response toward nitrite is imperative. Capillary electrophoresis,[5] spectrophotometry,[6] and ion chromatography,[7] *etc.* are useful with a high sensitivity, but there is a time-cost and more operation skills are required toward these analytical methods.[8,9] Of these above approaches, electrochemical determination has been widely developed owing to its extra merits, including real-time, low-cost, and feasibility.[10–14]

Metal–organic frameworks (MOFs) were constructed by assembling transition metal ions and organic linkers through coordination reactions. MOFs were firstly utilized for gas adsorption and storage application due to their porous structure and large surface area.[15] With the exploration of MOFs in the field of electrocatalysis, researchers found MOFs exposed more potential active sites on their larger surface, promoting easily the contact with target molecules, which further improved the electrocatalytic performance of MOFs,[16] making MOFs be perfect candidates for sensing.[17] However, great challenges remain for conventional MOFs due to their poor conductive/electronic properties, so the usage of MOFs in electrochemical applications is dramatically limited.[18–21]

To remove the above challenges, several strategies were put forward, such as (i) pyrolysis of MOFs, in which the carbonized MOFs possessed metal-doped or multi-atom-doped porous carbon, enhancing their electrocatalytic activity;[22,23] (ii) preparation of MOF-based hybrids, with conductive supports (carbon nanotube, graphene, metal foams, *etc.*) introduced for promoting their electrical conductivity;[24,25] (iii) synthesis of novel conductive MOFs, which can improve the electron transfer capacity directly without pre-treatments.[18,26] However, well-defined molecular active sites on MOFs are decomposed after the high-temperature process.[27] Also, the second method can promote their electrocatalytic activity to some extent, but it may reduce the inherent advantages of MOFs as well as decrease the surface area and reduce the accessible active sites. The third has more advantages over the other strategies, owing to the development of conductive MOFs, which can solve these challenges fundamentally and avoid the other approaches' negative effects.[26]

Two-dimensional (2D) conductive MOFs represent an emerging class of nanomaterials, presenting their exceptional 2D characteristics, enhanced ability of electron transfer and high efficiency of the active sites, as well as the intrinsic merits

[a]*Department of Agricultural and Biosystems Engineering, South Dakota State University, Brookings, South Dakota 57007, USA. E-mail: Hongxing.Jia@sdstate.edu; Zhengrong.Gu@sdstate.edu*

[b]*School of Engineering, Newcastle University, Newcastle Upon Tyne, NE1 7RU, UK*

[c]*Fraunhofer Center for Coatings and Diamond Technologies, Michigan State University, East Lansing, MI 48824, USA*

[d]*College of Chemistry and Chemical Engineering, Chongqing University of Technology, Chongqing 400054, People's Republic of China*

† Electronic supplementary information (ESI) available. See DOI: 10.1039/d0ra10522h

of conventional MOFs.[28] Such 2D conductive MOFs offer a perfect platform for the study of the mechanism of electroanalysis, which is helpful for the enhanced sensing performance of MOFs.[29] Recently, 2D Ni_3HHTP_2 ($HHTP_2$, hexahydroxytriphenylene) was synthesized for neurochemical detection due to a favorable electron transfer and large surface area.[30] 2D Cu-TCPP (TCPP, tetrakis(4-carboxyphenyl)porphyrin) modified with gold nanoparticles and polyxanthurenic acid with an exceptional conductivity was demonstrated as an excellent electrochemical sensor towards dopamine with a low detection limit.[31] 2D conductive materials also played an important role in gas analysis owing to their excellent conductivity.[29] Based on the above examples, 2D conductive MOFs present possibilities for achieving a superior electrocatalytic performance for electrochemical sensors.[31,32] However, the usage of 2D conductive MOFs in the electrochemical determination of small molecules has been rarely reported.

In this work, nickel phthalocyanine (NiPc) was selected as an organic linker to assemble a 2D NiPc-MOF. Three main reasons arise from using this linker for synthesizing a 2D MOF: (i) metal active sites are atomically dispersed on metal-lophthalocyanines, theoretically; (ii) NiPc-MOFs extend in two-dimension with fully in-plane π delocalization and weak out--of-plane π–π stacking, further promoting electron transfer between electrocatalysts and analytes; (iii) the larger surface area of a 2D NiPc-MOF, the easier absorption on the electrode, keeping its electrochemical stability, and then achieving an excellent sensitivity. Herein, a 2D conductive NiPc-MOF was synthesized through the solvothermal method and used for the electrochemical determination of nitrite for the first time.

The structural information of the as-prepared sample was explored by powder X-ray diffraction spectroscopy (PXRD), X-ray photoelectron spectroscopy (XPS), transmission electron microscopy (TEM) and atomic force microscopy (AFM). The XRD pattern of the sample in Fig. 1a exhibits peaks at 2θ = 4.15°, 9.85°, and 14.26°, indexed to the lattice planes of (200), (001), and (300), respectively. Long-range order within the *ab*-plane with a center-to-center (Ni···Ni) distance of 9.27 Å was further confirmed, which fits well with the simulation results of NiPc-MOF ($Ni_3(C_{32}H_{16}N_{16})_n$) (Fig. S1†) and no typical peaks of NiPc were found. XPS analysis indicates that the as-prepared sample is composed of Ni, C, N, and O. The Ni 2p spectrum exhibits the typical peaks for Ni $2p_{3/2}$ and Ni $2p_{1/2}$ at 854.6 eV peak 871.9 eV, respectively, which are the characteristic peaks of Ni(III) species (Fig. S2†).

The TEM image of the as-prepared sample exhibits it as an irregular shape with a nanosheet-like structure; several nanosheets are dispersed well in Fig. 1c. EDX spectrum of Fig. S3† further confirms its chemical content, including carbon, nitrogen, oxygen and nickel. The AFM (Fig. 1d) image of the sample exhibits its rough surface, and the corresponding height profile (Fig. S4†) reveals its thickness, ranging from 50 nm to 100 nm, indicating the as-prepared sample possesses a multi-layered structure. Furthermore, the FT-IR spectrum of the as-prepared sample (Fig. S5†) presents typical vibration absorptions of the basic building unit (NiPc) that three peaks at *ca.* 1628 cm^{-1}, 1552 cm^{-1} and 1114 cm^{-1} assigned to C=N stretching, C=C stretching and C–H bending, respectively. Nitrogen adsorption–desorption isotherms of NiPc-MOF nanosheets were performed at 77 K (Fig. S6†). The surface area of the NiPc-MOF nanosheets is 543 $m^2\ g^{-1}$, which is a little smaller than we previously reported.[26] Combined with the above analysis, it is demonstrated that we have successfully synthesized NiPc-based MOF (NiPc-MOF) nanosheets with both 2D features and typical MOF characteristics.

The electrocatalytic performance of the NiPc-MOF electrode towards nitrite was studied, as illustrated in Fig. 2. Fig. 3a shows cyclic voltammogram (CV) curves of the NiPc-MOF electrode in 0.1 M phosphate-buffered saline (PBS, pH 7.0) solution with/without 1.0 M nitrite. It can be found that the current response of the NiPc-MOF electrode increases sharply with the addition of nitrite compared to its response in the blank experiment. This means it is possible to achieve nitrite sensing on the surface of the NiPc-MOF electrode. To verify the NiPc-MOF electrode's feasibility, a series of nitrite solutions with different concentrations (0.35–0.75 M) was added into the test system, as shown in Fig. 3b. The result exhibits that the relationship of the current response *versus* concentration is clearly linear with a *c*-efficient value of 0.9998 (Fig. 3c). It demonstrates that the NiPc-MOF electrode has the potential to realize nitrite determination.

Under the optimal conditions (Fig. S7 and S8†), the electrochemical sensing of the NiPc-MOF electrode for nitrite

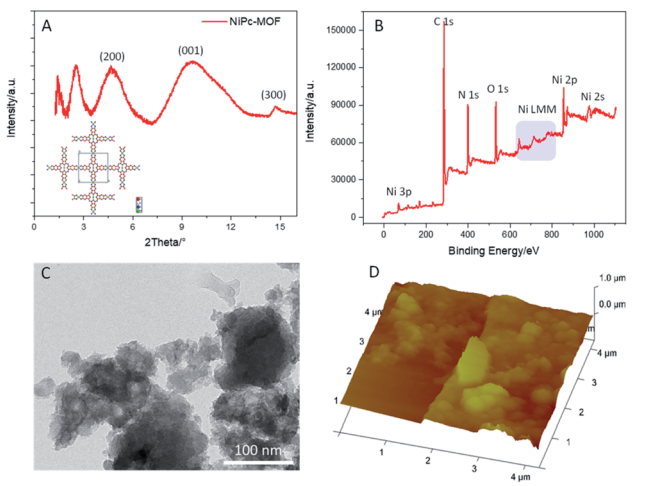

Fig. 1 (a) The PXRD pattern of NiPc-MOF and its predicted structure; (b) the XPS survey spectrum, (c) a TEM image, and (d) an AFM image of 2D NiPc-MOF nanosheets.

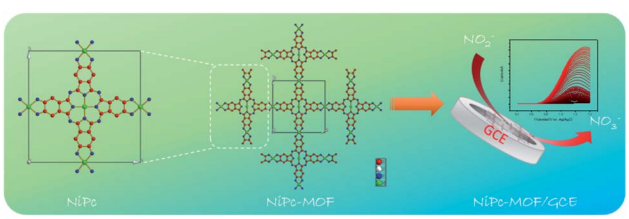

Fig. 2 A schematic diagram of the preparation of 2D NiPc-MOF and its use in electrochemical nitrite detection.

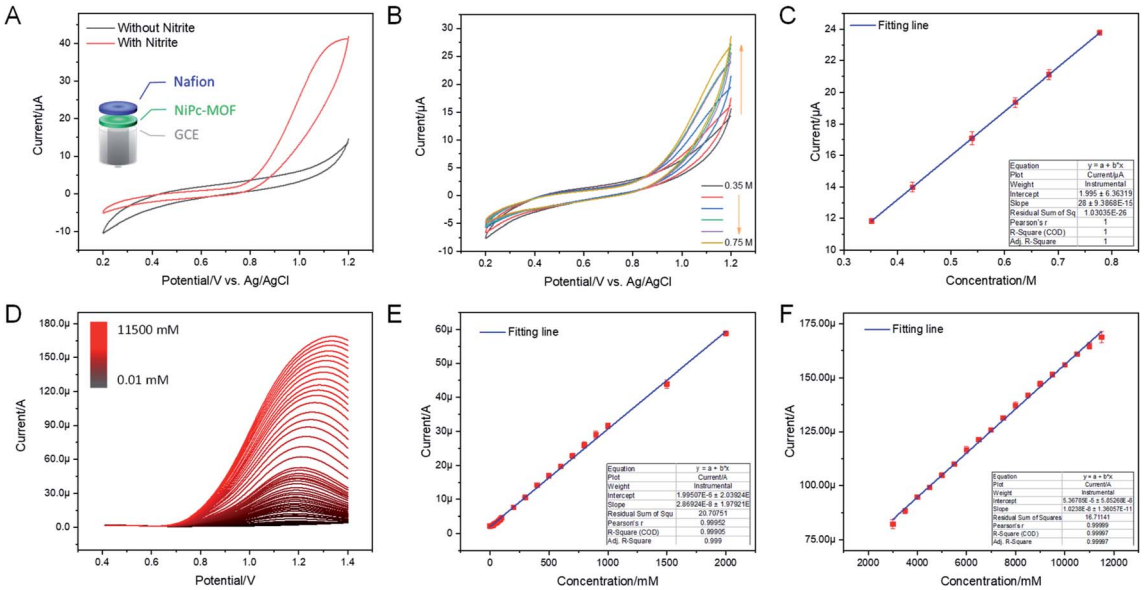

Fig. 3 (a) CV curves of the NiPc-MOF electrode in 1.0 M PBS buffer (pH 7.0) in the presence and absence of nitrite. (b) CV curves of the NiPc-MOF electrode at different nitrite concentrations (0.35–0.75 M), scan rate: 50 mV s^{-1}. (c) The linear calibration curve from the data in (b), concentration range: 0.35–0.75 M. (d) DPV curves of the 2D NiPc-MOF electrode during nitrite detection with successive additions (0.01–11 500 mM), DPV parameters: amplitude, 0.05 V; pulse width, 0.2 s; sampling width, 0.067 s; pulse period, 0.5 s. (e) The linear calibration curve from the data in (d) (concentration range: 0.01–2000 mM). (f) The linear calibration curve from the data in (d) (concentration range: 2500–11 500 mM).

oxidation was carried out by a differential pulse voltammogram (DPV). Fig. 3d presents the DPV curves at the NiPc-MOF electrode by the successive adding of nitrite with various concentrations from 0.01 mM to 11 500 mM. Each DPV curve can be completed within 6 s, exhibiting a fast response toward nitrite sensing. Fig. 3e and f display clearly linear curves between the current response of NiPc-MOF electrode and nitrite concentration with the regression equations: (i) $I/\mu A = 1.995 + 0.028 \times c$ ($R^2 = 0.999$, inset of Fig. 2f), (ii) $I/\mu A = 53.67 + 0.01 \times c$ ($R^2 = 0.9999$, inset of Fig. 3f). The sensitivity of the NiPc-MOF electrode is calculated as 0.40 μA mM^{-1} cm^{-2} and 0.14 A mM^{-1} cm^{-2} at low (0.01–2000 mM) and high concentrations (2500–11 500 mM), respectively. Then, a limit of detection (LOD) is estimated as 2.3 μM at a signal to noise ratio of 3 (S/N = 3). Additionally, the sensitivity of the NiPc-MOF electrode is slightly greater in the low concentrations from 0.01 to 2000 mM. This phenomenon can be explained as (i) all nitrite ions absorbed on the surface of the NiPc-MOF electrode; (ii) enough active sites on the NiPc-MOF electrode can catalyze them efficiently at a low concentration region. However, the electrocatalytic process is influenced by the competitive effects, including nitrite adsorption and catalytic activation on the surface of the NiPc-MOF electrode as the concentration increased, finally decreasing in sensitivity. As well, it is noted that the oxidation peak current appears slightly unstable when the nitrite concentration is beyond 2000 mM. This may be attributed to the adsorption saturation of NO_2^- on the active sites of the NiPc-MOF electrode. Compared with recent literature (Table S1†), the sensing performance of the NiPc-MOF electrode presents a very quick response, low LOD and ultrawide linear range (0.01–11 500 mM).

As shown in Fig. 4a, CV measurements of the NiPc-MOF electrode were studied in an electrochemical probe solution (5.0 mM ferricyanide and 0.1 M KCl); the NiPc electrode was employed for comparison. It was clearly found that the NiPc-MOF electrode has a larger closed curve area than that of the NiPc electrode. This phenomenon means NiPc-MOF nanosheets have a better electrical conductivity and faster electron transfer during electrochemical redox. EIS measurements

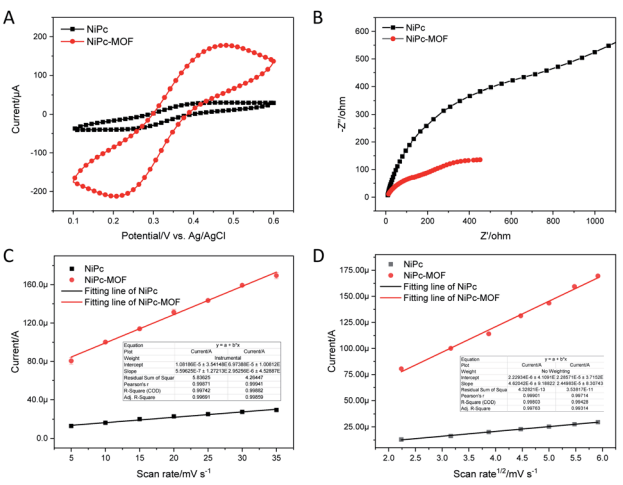

Fig. 4 (a) CV curves of the NiPc electrode and the 2D NiPc-MOF electrode in 1.0 mM ferricyanide with 0.1 M KCl, scan rate: 50 mV s^{-1}. (b) Nyquist plots of the NiPc electrode and the NiPc-MOF electrode in 1.0 mM ferricyanide containing 0.1 M KCl. (c) Electrochemical capacitance of the NiPc and NiPc-MOF electrodes. (d) The linear relationship between the oxidation peak currents and the square roots of the scan rates.

provide valuable information about the interfacial properties of the modified electrode. Fig. 4b reveals the Nyquist plots of the NiPc and NiPc-MOF electrodes, which exhibit semicircles at the high frequency range corresponding to the electron-transfer-limited process and a straight line at the low frequency range corresponding to the diffusion-limited process.[33] Then, Randle's equivalent circuit (Fig. S9†) was employed to simulate the obtained Nyquist plots, and further understand the electrical properties of the modified electrodes. The electron charge transfer resistance (R_{ct}) could be obtained based on the semicircle diameter of the Nyquist plots. The value of R_{ct} (803.8 Ω) of the conductive NiPc-MOF electrode was much smaller than that of the NiPc electrode (1680 Ω), indicating that the NiPc-MOF electrode brought a better conductivity to the electrode surface. The acceleration of the electron transfer rate was ascribed to the excellent conductivity of 2D NiPc-MOF nanosheets.

Generally, the double-layer capacitance (C_{dl}) was utilized to evaluate the modified electrode's active surface area. As shown in Fig. 4c, the effective active sites of the NiPc-MOF electrode for nitrite oxidation are obviously more than those of the NiPc electrode because the C_{dl} of that NiPc-MOF electrode is five times larger than that of the NiPc electrode (4.45 μF cm^{-2}). Moreover, the electrochemical active surface area of the modified electrode also reveals a transferred electron on the surface of the electrode and determines the active sites for nitrite oxidation.[12,34] As presented in Fig. 4d and S10,† there is a good linear relationship between the oxidation peak current (I_{pa}) and the square root of the scan rate ($\nu^{1/2}$). Therefore, the electrochemical active surface area could be determined as stated by the Randles–Sevcik eqn (1)[35]

$$I_{pa} = (2.69 \times 10^5) n^{3/2} A D^{1/2} \nu^{1/2} C_0 \quad (1)$$

In eqn (1), n, A, C_0, D, and ν are the number of transferred electrons, the surface area of the working electrode, reactant concentration, diffusion coefficient, and scan rate, respectively. Based on the known information, the electrochemical active surface area for NiPc-MOF electrode is 5.31 times larger than that of NiPc electrode. Consequently, the NiPc-MOF electrode is favorable for nitrite sensing due to the more sensitive response, higher charge transfer efficiency, more catalytic sites and increased electrochemically active surface area.

To verify the feasibility of the sensor, the fabricated sensor was utilized to monitor nitrite in real samples (tap water, and 0.1 M PBS were employed here for comparison) through a standard addition method. From the analysis results (Table S2†), the recovery values of real samples by the electrochemical method in this work were between 93.6% and 101.6%, and the RSD was less than 5%. To confirm the accuracy of the proposed method, a 0.1 M standard PBS solution was selected to detect the spiked samples, and the results are consistent with those of our proposed method, suggesting the approach is reliable for nitrite sensing in an actual complex environment.

An excellent selectivity is also an important standard for the prepared sensor, so the effect of interfering species, which possibly coexists with nitrite, on the response of the sensor was

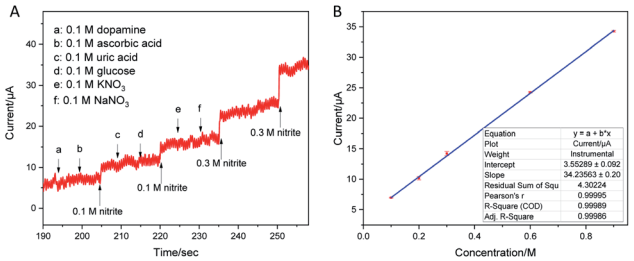

Fig. 5 (a) Amperometry curve of the NiPc-MOF electrode in 0.1 M PBS (pH 7.5) with successive additions of dopamine, ascorbic acid, uric acid, glucose, KNO_3, and $NaNO_3$ (all concentrations of the interfering species are 0.1 M) at an applied potential of 0.9 V. (b) The linear calibration curve of the data from (a) in the presence of interfering species.

assessed. Fig. 5a shows the interference measurement at the applied potential of 0.9 V with continuous additions of 0.1 M nitrite, 0.1 M dopamine, 0.1 M ascorbic acid, 0.1 M uric acid, 0.1 M glucose, 0.1 M KNO_3, 0.1 M $NaNO_3$ and 0.3 M $NaNO_2$ in 0.1 M PBS (pH 7.5). Obviously, a clear i–t response increase is revealed by the injection of 0.1 M nitrite into the blank buffer solution. In comparison with the response of NO_2^-, the i–t responses of other interfering species on the sensor were negligible. This phenomenon may be due to the specific electrocatalytic activity toward nitrite. In addition, as shown in Fig. 5b, the calibration curve of Fig. 5a exhibits a good linearity with a co-efficient value of 0.9998. The TEM image of the NiPc-MOF nanosheets after nitrite detection is presented in Fig. S11,† keeping the original morphological structure. This result confirms that the NiPc-MOF electrode possesses a great selectivity for the electrochemical detection of nitrite in the presence of multi-interfering species.

In addition, the repeatability of the as-prepared sensor was also investigated. Five individual electrodes were selected to study the repeatability of the NiPc-MOF electrode here. Five individual electrodes (#1–5) were prepared in the same conditions and applied to detect 0.1 M nitrite; the relative standard deviation (RSD) value was estimated to be 1.65%. As shown in Fig. 6a, the repeatability of the sensor was evaluated with 5 electrodes for detecting 0.1 M nitrite with a low RSD value (1.65%). As displayed in Fig. 6b, the peak current response of

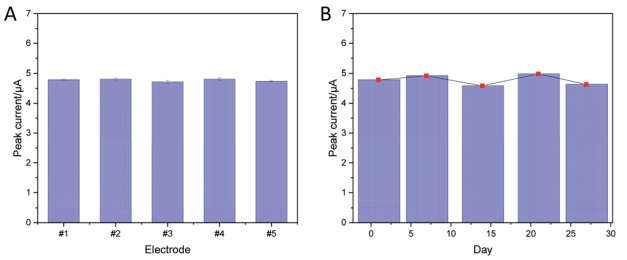

Fig. 6 (a) The repeatability of NiPc-MOF electrodes (#1–5) in 0.1 M PBS (pH 7.5) containing 0.1 M nitrite. (b) The stability of a NiPc-MOF electrode: peak current of DPV in 0.1 M PBS (pH 7.5) containing 0.1 M nitrite. DPV parameters: amplitude, 0.05 V; pulse width, 0.2 s; sampling width, 0.067 s; pulse period, 0.5 s.

the NiPc-MOF electrodes has a similar behavior over stability tests, the NiPc-MOF electrode was stored in an ambient environment and monitored every week *via* the DPV method. The RSD value of 3.82% was obtained, suggesting the stability of the NiPc-MOF electrode is suitable for long-term nitrite detection. Therefore, all the results suggest the NiPc-MOF electrode is reliable for nitrite sensing due to its excellent stability, repeatability, and long-term repeatability.

Conclusions

In conclusion, a two-dimensional nickel phthalocyanine-based metal–organic framework nanosheet (2D NiPc-MOF) based non-enzymatic biosensor for the electrochemical detection of nitrite was developed for the first time. The as-prepared sensor exhibited an ultra-wide detection range (0.01–11 500 mM) with a low limit of detection (2.3 μM); meanwhile, it also presents excellent stability and competitive selectivity. The excellent electrocatalytic activity of the NiPc-MOF electrode can be explained *via* the following reasons: (i) NiPc-MOF nanosheets possess highly catalytic sites with a larger electrochemical active surface area for nitrite oxidation; (ii) the 2D characteristics of the NiPc-MOF nanosheets result in a large surface area that increases the active sites for nitrite detection; and (iii) differently from the semi-conductivity of NiPc molecular examples, NiPc-MOF nanosheets present excellent electrical conductivity, which could enhance the electron transfer, improving the sensitivity towards nitrite determination. Overall, the prepared 2D NiPc-MOF nanosheets have great potential in the field of electroanalysis.

Conflicts of interest

There are no conflict of interests.

Acknowledgements

This work is financed by the National Science Foundation (EPSCoR. No. OIA-1849206, South Dakota 2D Materials for Biofilm Engineering, Science and Technology Center, 2DBEST) and USDA-NIFA Hatch (No. SD00H618-16, SD00R680-19 NC1194). The authors would like to thank Miss Ailin Guo for assistance with FT-IR measurements.

Notes and references

1 C.-Y. Hou, L.-M. Fu, W.-J. Ju and P.-Y. Wu, *Chem. Eng. J.*, 2020, 125573.
2 M. Annalakshmi, S. Kumaravel, S.-M. Chen, P. Balasubramanian and T. Balamurugan, *Sens. Actuators, B*, 2020, **305**, 127387.
3 M. L. Sall, B. Fall, I. Diédhiou, M. Lo, A. K. D. Diaw, D. Gningue-Sall, N. Raouafi and M. Fall, *Chem. Afr.*, 2020, 1–14.
4 D. Zhu, Q. Zhen, J. Xin, H. Ma, L. Tan, H. Pang and X. Wang, *Sens. Actuators, B*, 2020, **321**, 128541.
5 S.-L. Lin, J.-W. Hsu and M.-R. Fuh, *Talanta*, 2019, **205**, 120082.
6 Y.-S. Li, C.-L. Zhao, B.-L. Li and X.-F. Gao, *Food Chem.*, 2020, 127151.
7 E. Murray, P. Roche, K. Harrington, M. McCaul, B. Moore, A. Morrin, D. Diamond and B. Paull, *J. Chromatogr. A*, 2019, **1603**, 8–14.
8 D. Li, T. Wang, Z. Li, X. Xu, C. Wang and Y. Duan, *Sensors*, 2020, **20**, 54.
9 S. Lu, M. Hummel, X. Wang, W. He, R. Pathak, X. Dong, H. Jia and Z. Gu, *J. Electrochem. Soc.*, 2020, **167**, 146517.
10 J. Chen, S. Pang, L. He and S. R. Nugen, *Biosens. Bioelectron.*, 2016, **85**, 726–733.
11 Y. Han, R. Zhang, C. Dong, F. Cheng and Y. Guo, *Biosens. Bioelectron.*, 2019, **142**, 111529.
12 S. Lu, M. Hummel, S. Kang and Z. Gu, *J. Electrochem. Soc.*, 2020, **167**, 046515.
13 S. Lu, Z. Gu, M. Hummel, Y. Zhou, K. Wang, B. B. Xu, Y. Wang, Y. Li, X. Qi and X. Liu, *J. Electrochem. Soc.*, 2020, **167**, 106509.
14 S. Lu, C. Yang and M. Nie, *J. Alloys Compd.*, 2017, **708**, 780–786.
15 M. K. Sahoo, A. K. Samantara and J. N. Behera, *Inorg. Chem.*, 2020, **59**, 12252–12262.
16 C.-S. Liu, J. Li and H. Pang, *Coord. Chem. Rev.*, 2020, **410**, 213222.
17 J. Ding, L. Zhong, X. Wang, L. Chai, Y. Wang, M. Jiang, T.-T. Li, Y. Hu, J. Qian and S. Huang, *Sens. Actuators, B*, 2020, **306**, 127551.
18 X. Ma, C. Pang, S. Li, Y. Xiong, J. Li, J. Luo and Y. Yang, *Biosens. Bioelectron.*, 2019, **146**, 111734.
19 N. Zhou, F. Su, C. Guo, L. He, Z. Jia, M. Wang, Q. Jia, Z. Zhang and S. Lu, *Biosens. Bioelectron.*, 2019, **123**, 51–58.
20 F. Cai, Q. Wang, X. Chen, W. Qiu, F. Zhan, F. Gao and Q. Wang, *Biosens. Bioelectron.*, 2017, **98**, 310–316.
21 L. Chai, Z. Hu, X. Wang, Y. Xu, L. Zhang, T. T. Li, Y. Hu, J. Qian and S. Huang, *Adv. Sci.*, 2020, **7**, 1903195.
22 X. Niu, Q. Shi, W. Zhu, D. Liu, H. Tian, S. Fu, N. Cheng, S. Li, J. N. Smith, D. Du and Y. Lin, *Biosens. Bioelectron.*, 2019, **142**, 111495.
23 X. Wang, A. Dong, Y. Hu, J. Qian and S. Huang, *Chem. Commun.*, 2020, **56**, 10809–10823.
24 K. Fu, R. Zhang, J. He, H. Bai and G. Zhang, *Biosens. Bioelectron.*, 2019, **143**, 111636.
25 S. Lu, M. Hummel, K. Chen, Y. Zhou, S. Kang and Z. Gu, *Electrochem. Commun.*, 2020, **114**, 106715.
26 H. Jia, Y. Yao, J. Zhao, Y. Gao, Z. Luo and P. Du, *J. Mater. Chem. A*, 2018, **6**, 1188–1195.
27 J. Guo, C.-Y. Lin, Z. Xia and Z. Xiang, *Angew. Chem., Int. Ed.*, 2018, **57**, 12567–12572.
28 J. Park, M. Lee, D. Feng, Z. Huang, A. C. Hinckley, A. Yakovenko, X. Zou, Y. Cui and Z. Bao, *J. Am. Chem. Soc.*, 2018, **140**, 10315–10323.
29 Z. Meng, R. M. Stolz and K. A. Mirica, *J. Am. Chem. Soc.*, 2019, **141**, 11929–11937.

30 M. Ko, L. Mendecki, A. M. Eagleton, C. G. Durbin, R. M. Stolz, Z. Meng and K. A. Mirica, *J. Am. Chem. Soc.*, 2020, **142**, 11717–11733.
31 Z. Qiu, T. Yang, R. Gao, G. Jie and W. Hou, *J. Electroanal. Chem.*, 2019, **835**, 123–129.
32 Z. Meng, R. M. Stolz, L. Mendecki and K. A. Mirica, *Chem. Rev.*, 2019, **119**, 478–598.
33 N. Wang, M. Lin, H. Dai and H. Ma, *Biosens. Bioelectron.*, 2016, **79**, 320–326.
34 S. Lu, M. Hummel, Z. Gu, Y. Gu, Z. Cen, L. Wei, Y. Zhou, C. Zhang and C. Yang, *Int. J. Hydrogen Energy*, 2019, **44**, 16144–16153.
35 S. Palanisamy, B. Thirumalraj and S.-M. Chen, *J. Electroanal. Chem.*, 2016, **760**, 97–104.